発表者氏名	論文タイトル名	発表誌名	巻号	ページ	出版年
Kato M, et al.	Frameshift mutations of the *ARX* gene in familial Ohtahara syndrome.	Epilepsia	印刷中	未確定	2010
Goto A, et al., Osaka H, et al.	Proteomic and histochemical analysis of proteins involved in the dying-back-type of axonal degeneration in the gracile axonal dystrophy (gad) mouse.	*Neurochem Int.*	54:	330-338	2009
Ogiwara I, et al., Osaka H, et al.	De novo mutations of voltage-gated sodium channel alphaII gene SCN2A in intractable epilepsies.	*Neurology.*	29;	1046-53.	(2009),
Osaka H, et al.	Mild phenotype in Pelizaeus-Merzbacher disease caused by a PLP1-specific mutation.	Brain Dev	doi:10.1016		(2009),
Tsuji M, et al., Osaka H.	A New Case of GABA Transaminase Deficiency Detected with Proton MR Spectroscopy.	J Inherit Metab Dis,	10.1007/s10545-009-9022-9		(2010)
秦健一郎	DNAメチル化の網羅的解析	医学のあゆみ	230	553-554	2009
Kobayashi, H., Yamada, K., Morita, S., Hiura, H., Fukuda, A., Kagami, M., Ogata, T., Hata, K., Sotomaru, Y. and Kono, T.	Identification of the mouse paternally expressed imprinted gene Zdbf2 on chromosome 1 and its imprinted human homolog ZDBF2 on chromosome 2.	*Genomics.*	93	461-472	2009

生体の科学：<< 特集　SNARE 複合体 - 膜融合の機構>>

12. *STXBP1* 遺伝子（MUNC18-1）のハプロ不全が難治性のてんかんを引き起こす

才津　浩智[1]、松本　直通[2]

[1]横浜市立大学　大学院医学研究科　遺伝学　助教

[2]横浜市立大学　大学院医学研究科　遺伝学　教授

Haploinsufficiency of the gene encoding MUNC18-1 cause intractable early infantile epilepsy

校正送付先

才津　浩智

横浜市立大学　大学院医学研究科

遺伝学 助教

〒236-0004 横浜市金沢区福浦 3-9

Tel: 045-787-2606, Fax: 045-786-5219

E-mail: hsaitsu@yokohama-cu.ac.jp

図は 1－4

てんかんは，大脳神経細胞の過剰な放電によって引き起こされる反復性の発作（てんかん発作）を主な徴候とする疾患である。脳奇形などの明らかな原因が認められる場合（症候性）と明らかな原因が認められない場合（特発性または潜因性）があり，後者において報告されている原因遺伝子の多くがイオンチャネルをコードしている。我々は，脳奇形のない，新生児から乳児期早期に発症する難治性のてんかん患者に，*STXBP1*遺伝子の新生突然変異を同定した。*STXBP1*遺伝子は，SNARE複合体の機能を調節することが知られているMUNC18-1タンパク質をコードしている。変異を有するMUNC18-1は構造的に不安定で，シンタキシン-1Aとの結合能が著しく低下していた[1)]。これらの所見は，シナプス小胞の開口放出障害という新しいてんかんの発症機構を強く示唆するものである。本稿では，*STXBP1*遺伝子変異の同定に至るゲノム解析，変異MUNC18-1の機能解析について概説する。

1．大田原症候群（early infantile epileptic encephalopathy with suppression burst：EIEE）

大田原症候群は，新生児期から乳児期早期に，頻回の短い単発性あるいはシリーズ形成性の全般性強直発作 (全身の筋肉を硬直させる発作)で発症し，重度の精神運動発達遅滞を伴う難治性のてんかんである。小児神経科医の大田原俊輔先生（岡山大学小児神経科初代教授）が 1976 年に世界にさきがけて疾患をまとめられた[2)]。脳波検査では，棘波/鋭波/徐波の混在する高振幅の burst と，低振幅でほぼ平坦な suppression が交互に出現する suppression burst パターンが，覚醒，睡眠時を問わず認められる[3,4)]。大田原症候群の多くは脳形成異常を伴うが，脳形成異常がない症例（潜因性）も認められ，遺伝的な素因が示唆されていた。これまで，X 染色体上に位置する *ARX* (aristaless related homeobox) 遺伝子変異が男児例において報告されているのみで[5)]，同定された責任遺伝子変異で原因が説明できない症例が多く残されていた。

2．全ゲノムマイクロアレイによる染色体構造異常の同定

大田原症候群のほとんどは弧発例で生殖適合性が低いため，従来の家系例を用いた連鎖解析では疾患遺伝子の単離が不可能であった。弧発例がメインである疾患においては，転座や欠失といった染色体構造異常を手がかりとしたポジショナルクローニング法が有効である。このアプローチの特徴は，１例の染色体異常から遺伝子単離が可能であることであり，当研究室ではこの手法を用いてマルファン症候群2型の原因遺伝子の同定に成功した[6)]。染色体構造異常を網羅的にスクリーニングするために，我々は全ゲノム解析用BACマイクロアレイを作製した。これは，ゲノムDNAを含むBAC (bacterial artificial chromosome) や PAC (P1-derived artificial chromosome) クローンDNAを，基盤となるスライドガラスに均等間隔にスポットしたものである。患者DNAと正常対照DNAを異なる蛍光色素で標識して同時に競合ハイブリダイゼーションさせ，そのシグナル強度比から患者DNAにおけるゲノムコピー数の変化を検出する。我々はこのBACマイクロアレイを用いて、大田原症候群の女児症例に第9染色体長腕（9q33.3-q34.11）の微細欠失を同定した（図１A)。白血球染色体標本

を用いた蛍光 *in situ* hybridization法により，ヘテロ接合性の約2.0Mbの欠失（2本ある相同染色体のうちどちらか一方で欠失がある）が患者のみに存在し，患者の両親では欠失が認められないことを確認した（図１B)。これらの結果は，染色体の微細欠失は患者に起こった新生突然変異であり，大田原症候群の原因となっている可能性が極めて高いことを意味した。

３．大田原症候群患者における *STXBP1* 遺伝子変異の同定

微細欠失の領域には，ヒト脳での発現が報告されていた *syntaxin binding protein 1* (*STXBP1*) 遺伝子を含めて 40 個以上の遺伝子が位置していた（図１B)。我々は，大田原症候群患者 13 名で *STXBP1* の変異解析を行い，４名でヘテロ接合性のミスセンス変異（遺伝子がコードするタンパク質にアミノ酸の置換をもたらす変異）を認めた（図 2)。これら４つの変異は対照健常人 250 名に認められず，3 変異については両親では認められない新生突然変異であることを確認した。1 変異については父親が他界しており，新生突然変異の確認ができなった。*STXBP1* 変異を有する患者は，核磁気共鳴画像法検査で脳形成異常を認めず，特徴的な suppression burst パターンの脳波を呈した。これらの所見から，*STXBP1* 変異が潜因性の大田原症候群の原因となっていると考えられた。

４．変異 MUNC18-1 タンパク質の機能解析

*STXBP1*遺伝子は，進化的に保存されたSec1/Munc-18 (SM)タンパク質ファミリーの１つであるMUNC18-1をコードしている[7,8]。SMタンパク質はSNAREタンパク質と同様に，酵母から哺乳類に至るすべての種で，生体膜融合に必須であることが知られている[9]。神経系では，前シナプス側の神経細胞が興奮し，活動電位が前シナプスに到達すると，神経伝達物質を蓄えているシナプス小胞が前シナプス膜に融合して神経伝達物質の開口放出が起こる。哺乳類では、小胞上のvesicle-SNAREであるVAMP2（シナプトブレビン2）と前シナプス膜上のtarget-SNAREsであるシンタキシン-1，SNAP-25 が結合して形成するSNARE 複合体の働きにより，シナプス小胞と前シナプス膜が融合する。この過程において，SNARE 複合体を制御するタンパク質の１つがMUNC18-1である[9]。MUNC18-1はシンタキシン-1Aと結合するタンパク質として発見され[10]，シンタキシン-1Aとの結合，あるいはSNARE 複合体に直接結合することにより，開口放出を調節していると考えられている[9,11]。シンタキシン-1Aは開放型と閉鎖型の２つの立体構造をとることが知られているが[12]，MUNC18-1は開放型と閉鎖型のどちらのシンタキシン-1Aとも結合する。開放型シンタキシン-1Aのアミノ末端への結合は膜融合に重要であり，閉鎖型シンタキシン-1Aとの結合はシナプス小胞のドッキングに関与している[9,11,13,14]。

大田原症候群患者で見つかったミスセンス変異によるアミノ酸の置換は，すべて多種間で高度に保存されたアミノ酸の置換をもたらす変異であった（図2)。また，MUNC18-1の立体構造上，内部に位置する疎水性アミノ酸で置換が生じており，立体構造を不安定に

することが予測された（図3A）。そこで我々は，正常型とC180Y変異型MUNC18-1を精製し，その構造と機能を解析した。円二色性スペクトラム実験では，αヘリックスの含量が正常型（43%）に比べてC180Y変異型（39%）で少なく，変異によりMUNC18-1の二次構造が変化していることが示唆された。さらに円二色性融解実験を行ったところ，C180Y変異型は正常型よりも熱に対して大幅に不安定であることが明らかになった（図3B）。また，シンタキシン-1Aとの結合能において，C180Y変異型は正常型と比べて，開放型シンタキシン-1A（L165A, E166A変異）との結合が著しく低下していた（図3C）。他の変異MUNC18-1（V84D, M443R, G544D）に関しても精製を試みたが，精製過程における凝集のため，十分な量が得られなかった。EGFPタグを付加したMUNC18-1をNeuroblastoma 2A細胞に一過性発現させ，EGFPの蛍光をもとに細胞内局在を検討した実験においても，患者で認められた4種類の変異をもつMUNC18-1は，約20%の発現細胞で凝集が認められた（図4）。これらの結果から，大田原症候群患者で認められたミスセンス変異は，MUNC18-1の立体構造を不安定化し，開放型シンタキシン-1Aとの結合能を著しく低下させることが明らかとなり、シナプス小胞の開口放出障害という新しいてんかんの発症機構が強く示唆された。

5．MUNC18-1のハプロ不全とてんかん

これまでに大田原症候群患者では，上述のヘテロ接合性の遺伝子欠失，ミスセンス変異のほかに，ヘテロ接合性のナンセンス変異，フレームシフト変異，スプライシング変異が見つかってきている（才津、投稿中）。見つかったフレームシフト変異，スプライシング変異はともに早期終止コドンを導入するため，ナンセンス変異の場合と同様に，RNA 監視機構の１つである「ナンセンス変異による mRNA 分解」を受けると予想される。また、C180Y 変異型 MUNC18-1 は不安定であり，開放型シンタキシン-1A との結合能を著しく低下させていることから，シナプス小胞の開口放出に関してはほぼ機能していないと考えられる。更に，ヘテロ接合性の遺伝子欠失で大田原症候群が生じていることを考えると，正常な MUNC18-1 の量が半分程度に低下すること（MUNC18-1 のハプロ不全）によって大田原症候群が生じていると結論づけられる。Mun18-1 ホモ変異マウスは，神経伝達物質の開口放出が全く認められず，呼吸ができずに生後すぐに死亡する[15]。Mun18-1 ヘテロ変異マウスにおけるてんかん発作の報告はなく，自己シナプス形成下での Mun18-1 ヘテロ変異ニューロンの電気生理学的所見も，標準的な条件下では正常型と比較して変化が認められない[16]。しかしながら，繰り返し刺激による後シナプス電流の抑制が Mun18-1 ヘテロ変異ニューロンで早期に起こることなどから，シナプス小胞の readily releasable pool size が減少していることが示唆されている[16]。興味深いことに，この readily releasable pool size の減少は，グルタミン酸作働性ニューロンに比べて GABA 作働性ニューロンにより強く認められている[16]。前述の *ARX* 遺伝子は，抑制性の GABA 作働性を含めた介在ニューロンの移動と分化を調節していることが知られており[17]，*ARX* 遺伝子変異によって引き起こされる介在ニューロンの異常がてんかんを引き起こしているという仮説（interneuorpathy）が提唱されている[18]。

*STXBP1*変異による影響が，ヒトにおいても介在ニューロンにより強く現れるなら，*STXBP1*変異がもたらすてんかんの病態に，介在ニューロンの機能不全が関与している可能性がある。

6．今後への期待

最近 Hamdan らは，精神発達遅滞と非症候群性のてんかんを呈する患者における*STXBP1*のヘテロ接合性新生突然変異（ナンセンス変異 1 例、スプライス変異 1 例）を報告した[19]。この報告は，*STXBP1*変異が，新生児期から乳児期早期に発症する難治性てんかんだけでなく、精神発達遅滞とてんかんをキーワードとした幅広い病気の原因となっていることを示唆している。今後，*STXBP1*変異の引き起こす表現型がどのような広がりを見せるのか注目したい。また、特発性てんかんの原因遺伝子の多くがイオンチャネルをコードしており，シナプス小胞の開口放出に関与する遺伝子としては，これまでにシナプシン 1 の遺伝子変異がてんかんと学習障害を呈する 1 家系で報告されているのみであった[20]。*STXBP1*変異の発見によって，シナプス小胞の開口放出に関わる遺伝子のてんかんへ明確な関与が明らかになり，今後シナプス小胞の開口放出に関わる遺伝子とてんかんに関する研究が進むことを期待したい。

文献

1. Saitsu H, Kato M, Mizuguchi T et al : *Nat Genet.* **40**: 782-8, 2008
2. 大田原俊輔，石田喬士、岡鍥次ほか ： 脳と発達 8 : 270-279, 1976
3. Ohtahara S, Yamatogi Y : *Epilepsy Res.* **70 Suppl 1**: S58-67, 2006
4. Djukic A, Lado FA, Shinnar S et al : *Epilepsy Res.* **70 Suppl 1**: S68-76, 2006
5. Kato M, Saitoh S, Kamei A et al: *Am J Hum Genet.* **81**: 361-366, 2007
6. Mizuguchi T, Collod-Beroud G, Akiyama T et al. : *Nat Genet.* **36**: 855-860, 2004
7. Sudhof TC : *Annu Rev Neurosci.* **27**: 509-47, 2004
8. Weimer RM, Richmond JE : *Curr Top Dev Biol.* **65**: 83-113, 2005
9. Toonen RF, Verhage M : *Trends Neurosci.* **30**: 564-72, 2007
10. Hata Y, Slaughter CA, Sudhof TC: *Nature.* **366**: 347-51, 1993
11. Dulubova I, Khvotchev M, Liu S et al: *Proc Natl Acad Sci U S A.* **104**: 2697-702, 2007
12. Dulubova I, Sugita S, Hill S et al: *EMBO J.* **18**: 4372-82, 1999
13. Rickman C, Medine CN, Bergmann A et al: *J Biol Chem.* **282**: 12097-103, 2007
14. Shen J, Tareste DC, Paumet F et al: *Cell.* **128**: 183-195, 2007
15. Verhage M, Maia AS, Plomp JJ et al: *Science.* **287**: 864-9, 2000
16. Toonen RF, Wierda K, Sons MS et al: *Proc Natl Acad Sci U S A.* **103**: 18332-7, 2006
17. Kitamura K., Yanazawa M., Sugiyama N et al: *Nat Genet.* **32**: 359-69, 2002
18. Kato M, Dobyns WB : *J Child Neurol.* **20**: 392-7, 2005

19. Hamdan FF, Piton A, Gauthier J et al: *Ann Neurol.* **65**: 748-53, 2009
20. Garcia CC, Blair HJ, Seager M et al: *J Med Genet.* **41**: 183-6, 2004

図の説明

図 1 大田原症候群患者で認めた染色体の微細欠失

(A) 染色体微細欠失を同定した全ゲノム解析用 BAC マイクロアレイの結果を示す。CGH1 は患者 DNA を Cy5 蛍光色素で、対照健常人 DNA を Cy3 蛍光色素でラベルしており、CGH2 では蛍光色素を交換してラベルしている。Log_2（Cy5 と Cy3 の蛍光強度の比）の値を縦軸に、9 番染色体の短腕から長腕にかけての各 BAC クローンの位置を横軸に示す。この症例では長腕に CGH1 でマイナスに、CGH2 でプラスに値が大きくなる領域(赤い Box)があり、染色体の欠失と考えられた。(B) BAC クローンをラベルしてプローブとした蛍光 *in situ* hybridization 法により、9q33.3-q34.11 にかけて約 2.0Mb の欠失領域を同定した。紫色のクローンが欠失領域に位置するクローンを、写真の矢印が欠失した染色体領域を示す。この欠失領域には 41 個の遺伝子が存在していた。

図 2 大田原症候群患者で認めた *STXBP1* 遺伝子のヘテロ接合性ミスセンス変異

同定された 4 つの塩基置換は機能ドメイン内でのアミノ酸置換を引き起こす。変異は多種間で進化的に高度に保存されたアミノ酸で生じており、4 つのうち 3 つの変異については御両親に変異がない新生突然変異であった。

図 3 変異タンパク質の構造及び機能解析

(A) 変異により MUNC18-1 タンパク質の内部に位置する疎水性アミノ酸で置換が生じている。(B) 円偏光二色性融解実験による熱安定性の評価では、変異タンパク質（p.C180Y）が正常型（WT）に比べて熱安定性が著しく低下していることが分かった。(C) 変異タンパク質は正常型と比べて開放型シンタキシン-1A との結合能が著しく低下していた。

図 4 Neuroblastoma 2A 細胞における正常および変異 MUNC18-1 タンパク質の強制発現

コントロールの EGFP-C1（EGFP のみ）は細胞全体に存在しているのに対して、EGFP と MUNC18-1 (WT) との融合タンパク質は細胞核を除いた細胞質全体に存在している。一方、4 種類の変異 MUNC18-1 と EGFP の融合タンパク質は、細胞内で強く凝集しているのが観察された。サンプル間の比較のため、蛍光画像は露光時間を固定して取り込んだ。

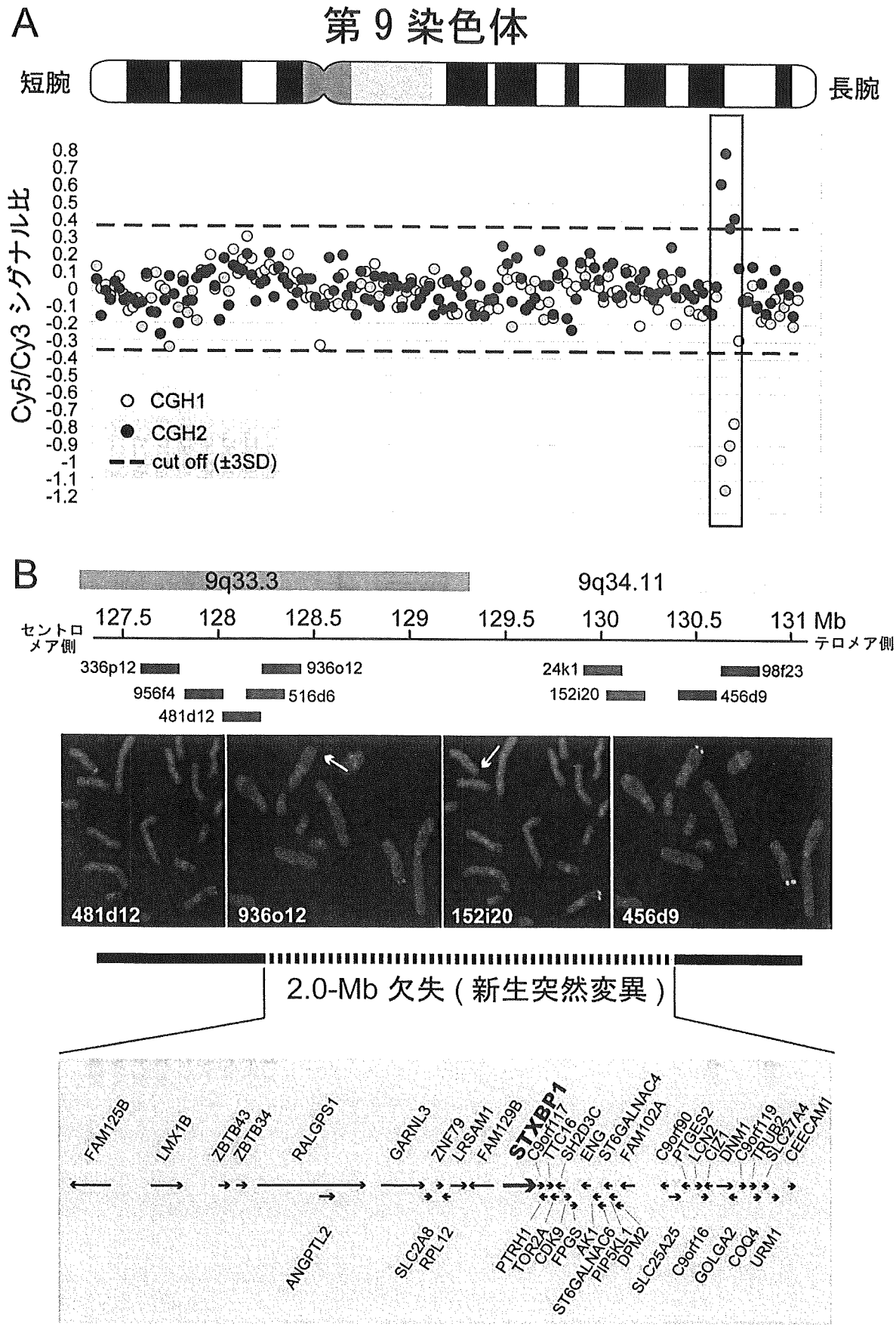
A
第 9 染色体
短腕
長腕
Cy5/Cy3 シグナル比
0.8
0.7
0.6
0.5
0.4
0.3
0.2
0.1
0
-0.1
-0.2
-0.3
-0.4
-0.5
-0.6
-0.7
-0.8
-0.9
-1
-1.1
-1.2
CGH1
CGH2
cut off (±3SD)
B
9q33.3
9q34.11
セントロメア側
127.5
128
128.5
129
129.5
130
130.5
131 Mb
テロメア側
336p12
936o12
956f4
516d6
481d12
24k1
98f23
152i20
456d9
481d12
936o12
152i20
456d9
2.0-Mb 欠失 (新生突然変異)
FAM125B
LMX1B
ZBTB43
ZBTB34
RALGPS1
GARNL3
ZNF79
LRSAM1
FAM129B
STXBP1
C9orf117
TTC16
SH2D3C
ENG
ST6GALNAC4
FAM102A
C9orf90
PTGES2
LCN2
CIZ1
DNM1
C9orf119
TRUB2
SLC27A4
CEECAM1
ANGPTL2
SLC2A8
RPL12
PTRH1
TOR2A
CDK9
FPGS
AK1
ST6GALNAC6
PIP5KL1
DPM2
SLC25A25
C9orf16
GOLGA2
COQ4
URM1

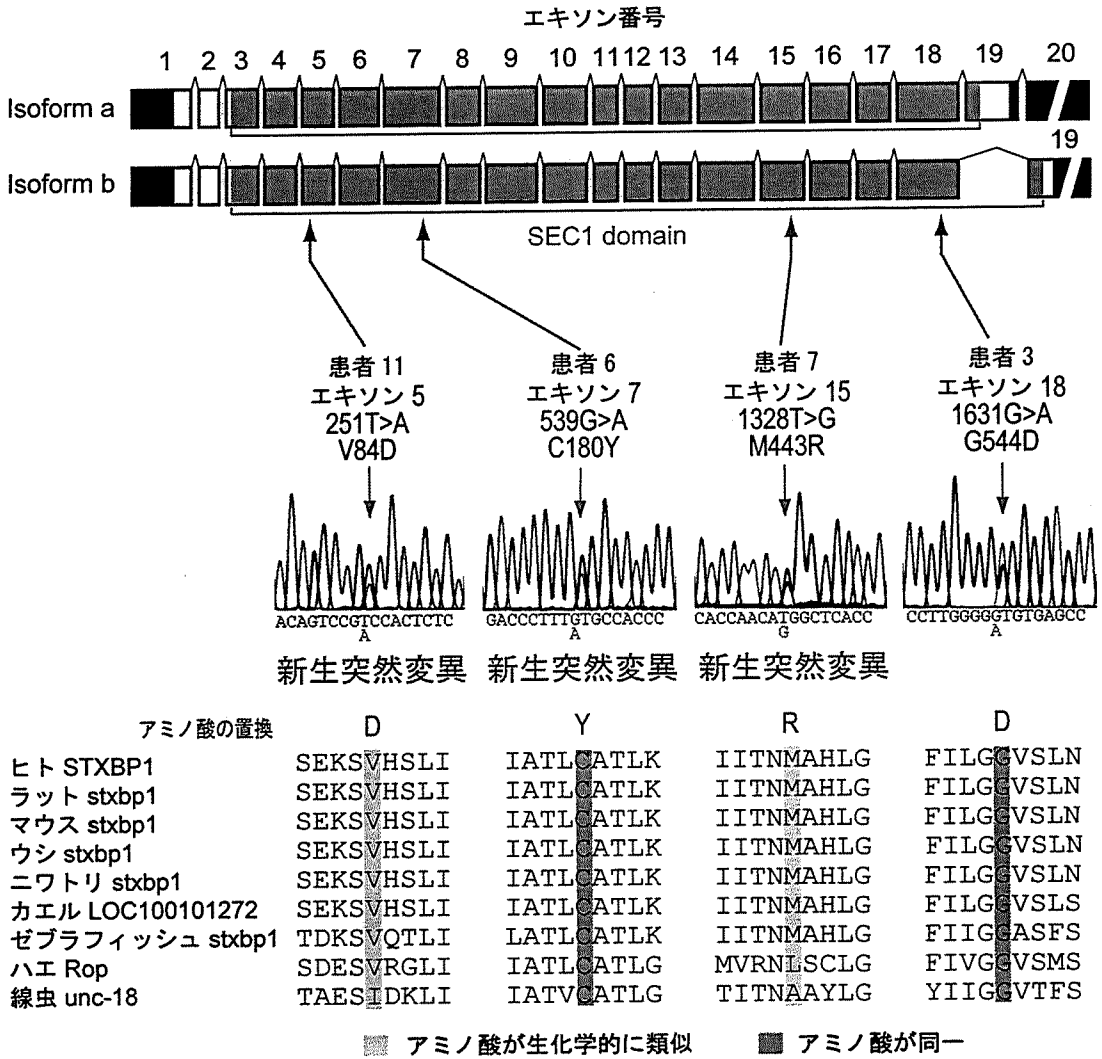
エキソン番号
1 2 3 4 5 6 7 8 9 10 11 12 13 14 15 16 17 18 19 20
Isoform a
19
Isoform b
SEC1 domain
患者 11
エキソン 5
251T>A
V84D
患者 6
エキソン 7
539G>A
C180Y
患者 7
エキソン 15
1328T>G
M443R
患者 3
エキソン 18
1631G>A
G544D
ACAGTCCGTCCACTCTC
A
GACCCTTTGTGCCACCC
A
CACCAACATGGCTCACC
G
CCTTGGGGGTGTGAGCC
A
新生突然変異 新生突然変異 新生突然変異
アミノ酸の置換 D Y R D
ヒト STXBP1 SEKSVHSLI IATLCATLK IITNMAHLG FILGGVSLN
ラット stxbp1 SEKSVHSLI IATLCATLK IITNMAHLG FILGGVSLN
マウス stxbp1 SEKSVHSLI IATLCATLK IITNMAHLG FILGGVSLN
ウシ stxbp1 SEKSVHSLI IATLCATLK IITNMAHLG FILGGVSLN
ニワトリ stxbp1 SEKSVHSLI IATLCATLK IITNMAHLG FILGGVSLN
カエル LOC100101272 SEKSVHSLI IATLCATLK IITNMAHLG FILGGVSLS
ゼブラフィッシュ stxbp1 TDKSVQTLI LATLCATLK IITNMAHLG FIIGGASFS
ハエ Rop SDESVRGLI IATLCATLG MVRNLSCLG FIVGGVSMS
線虫 unc-18 TAESIDKLI IATVCATLG TITNAAYLG YIIGGVTFS
アミノ酸が生化学的に類似
アミノ酸が同一

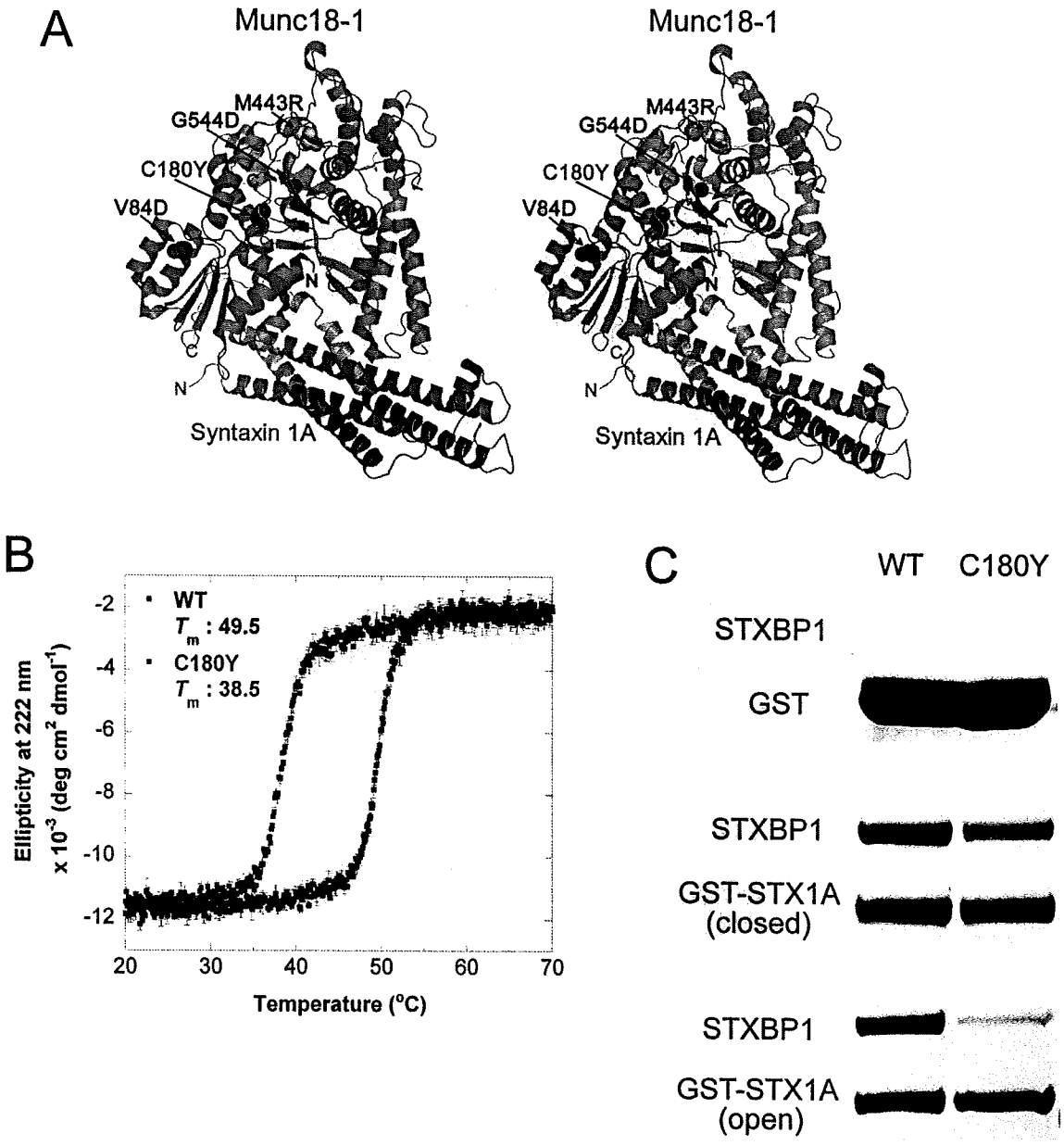
A
Munc18-1
M443R
G544D
C180Y
V84D
N
N
Syntaxin 1A
Munc18-1
M443R
G544D
C180Y
V84D
N
C
N
Syntaxin 1A
B
WT
T_m : 49.5
C180Y
T_m : 38.5
Ellipticity at 222 nm
x 10^{-3} (deg cm^2 dmol^{-1})
-2
-4
-6
-8
-10
-12
20
30
40
50
60
70
Temperature (°C)
C
WT
C180Y
STXBP1
GST
STXBP1
GST-STX1A
(closed)
STXBP1
GST-STX1A
(open)

EGFP-C1
WT
V84D
C180Y
M443R
G544D

ARTICLE

Zebrafish Gene Knockdowns Imply Roles for Human *YWHAG* in Infantile Spasms and Cardiomegaly

Yuta Komoike,[1] Katsunori Fujii,[2] Akira Nishimura,[3,4] Yoko Hiraki,[5] Michiko Hayashidani,[6] Keiko Shimojima,[1] Tsutomu Nishizawa,[1] Kouji Higashi,[2] Kumi Yasukawa,[2] Hirotomo Saitsu,[3] Noriko Miyake,[3] Takeshi Mizuguchi,[3] Naomichi Matsumoto,[3,4,7] Makiko Osawa,[8] Yoichi Kohno,[2] Toru Higashinakagawa,[9] and Toshiyuki Yamamoto[1]*

[1]International Research and Educational Institute for Integrated Medical Sciences (IREIIMS), Tokyo Women's Medical University, Tokyo, Japan
[2]Department of Pediatrics, Graduate School of Medicine, Chiba University, Chiba, Japan
[3]Department of Human Genetics, Graduate School of Medicine, Yokohama City University, Yokohama, Japan
[4]21st Century Center of Excellence (COE) Program of MEXT, The Yokohama City University, Yokohama, Japan
[5]Hiroshima Municipal Center for Child Health and Development, Hiroshima, Japan
[6]Medical Center for Premature and Neonatal Infants, Hiroshima City Hospital, Hiroshima, Japan
[7]Solution-Oriented Research for Science and Technology, Japan Science and Technology Agency, Tokyo, Japan
[8]Department of Pediatrics, Tokyo Women's Medical University, Tokyo, Japan
[9]Department of Biology, School of Education, Waseda University, Tokyo, Japan

Received 7 May 2009; Revised 21 December 2009; Accepted 28 December 2009

Summary: Williams-Beuren syndrome (WBS) is a neurodevelopmental disorder presenting with an elfin-like face, supravalvular aortic stenosis, a specific cognitive-behavioral profile, and infantile hypercalcemia. We encountered two WBS patients presenting with infantile spasms, which is extremely rare in WBS. Array comparative genomic hybridization (aCGH) and fluorescent in situ hybridization (FISH) analyses revealed atypical 5.7-Mb and 4.1-Mb deletions at 7q11.23 in the two patients, including the WBS critical region and expanding into the proximal side and the telomeric side, respectively. On the proximal side, *AUTS2* and *CALN1* may contribute to the phenotype. On the telomeric side, there are two candidate genes *HIP1* and *YWHAG*. Because detailed information of them was unavailable, we investigated their functions using gene knockdowns of zebrafish. When zebrafish *ywhag1* was knocked down, reduced brain size and increased diameter of the heart tube were observed, indicating that the infantile spasms and cardiomegaly seen in the patient with the telomeric deletion may be derived from haploinsufficiency of *YWHAG*. genesis 00:1–11, 2010. © 2010 Wiley-Liss, Inc.

Key words: Williams-Beuren syndrome (WBS); infantile spasms; cardiomegaly; *YWHAG*; *HIP1*; developmental delay; array comparative genomic hybridization (aCGH); fluorescent in situ hybridization (FISH); 7q11.23; microdeletion

INTRODUCTION

William-Beuren syndrome (WBS) is a recognizable malformation syndrome (MIM: 194050) (http://www.ncbi.nlm.nih.gov/Omim/) caused by hemizygosity of chromosome 7q11.23 (Ewart *et al.*, 1993). WBS patients show mental retardation with a specific cognitive-behavioral profile, supravalvular aortic stenosis, infantile hypercalcemia, a hoarse voice, and distinctive dysmorphic features including an elfin-like face and edematous eyes. The prevalence of WBS in the population is approximately one in 7,500–20,000 (Ewart *et al.*, 1993; Stromme *et al.*, 2002; Wu *et al.*, 1998). Almost all deletions of 7q11.23 in patients with WBS have arisen by de novo mechanisms. The phenotypes of WBS patients are caused by haploinsufficiency of the contiguous genes included in approximately 1.5 Mb or 1.9 Mb regions of 7q11.23, which is mediated by flanking low-copy repeats (LCRs), and are common among WBS patients (Morris, 2006). More than 20 genes are located within this common deletion region, including the elastin gene (*ELN*), the most important gene for the cardiovascular changes associated with WBS (Morris, 2006). Nucleotide sequence alterations in *ELN* can cause isolated supravalvular aortic stenosis (Morris, 2006).

Additional Supporting Information may be found in the online version of this article.

*Correspondence to: Toshiyuki Yamamoto, International Research and Educational Institute for Integrated Medical Sciences (IREIIMS), Tokyo Women's Medical University, 8-1 Kawada-cho, Shinjuku-ward, Tokyo 162-8666, Japan. E-mail: yamamoto@imcir.twmu.ac.jp

Contract grant sponsors: Program for Promoting the Establishment of Strategic Research Centers, Special Coordination Funds for Promoting Science and Technology, Ministry of Education Culture, Sports, Science and Technology (Japan).
Published online in
Wiley InterScience (www.interscience.wiley.com).
DOI: 10.1002/dvg.20607

Patients with uncommon deletion sizes that also show atypical phenotypes are of particular interest to researchers for assessment of genotype–phenotype comparisons. WBS patients with common deletions rarely have epilepsy, especially infantile spasms. Until now, only a few WBS patients with infantile spasms have been reported (Mizugishi *et al.*, 1998; Morimoto *et al.*, 2003). In 2008, Marshall *et al.* reported 28 patients with infantile spasms, twenty of whom had deletion of 7q11.23, the WBS critical region, and eight of whom had deletion of 7q21. A genotype-phenotype analysis localized the shortest region of overlap to membrane associated guanylate kinase, ww and pdz domains-containin, 2 gene (*MAGI2*), located in the telomeric region outside of the WBS critical region (Marshall *et al.*, 2008). However, some WBS patients with infantile spasms had no deletion in *MAGI2*, and some patients with haploinsufficiency of *MAGI2* did not have infantile spasms. Thus, there may be other genes in this region that are responsible for infantile spasms.

Recently, we encountered two WBS patients, both of whom presented with infantile spasms, and one of whom also presented with cardiomegaly. Array comparative genomic hybridization (aCGH) showed that the 7q11 deletions in these patients are larger than the common WBS deletion, but do not include *MAGI2*. Thus, we investigated genes that might be responsible for such atypical phenotypes.

RESULTS

Patient Profiles

Patient 1. A boy was born at 41 weeks of gestation as a second child between an unrelated 33-year-old father and 31-year-old mother without any familial history. His birth weight was 2,892 g, length was 49 cm, and head circumference was 33 cm. He was transferred to the neonatal intensive care unit (NICU) because of poor sucking. He was suspected of WBS at one month, and fluorescent in situ hybridization (FISH) analysis confirmed a deletion in 7q11.23 (data not shown). Infantile spasm occurred at four months. An electroencephalogram revealed hypsarrhythmia. He was referred to us for evaluation of development. Specific facial features were noted, including wide forehead, broad eyebrows, downslanting palpebral fissures, inverted epicanthus, periorbital fullness, low-set ears with prominent lobes, short nose, full nasal tip, malar hypoplasia, long philtrum, thick lips, high arched palate, full cheeks, and micrognathia. Echocardiography revealed supravalvular aortic stenosis and peripheral pulmonary stenosis. Bilateral radioulnar synostosis, joint laxity, soft skin, bilateral inguinal hernia, left cryptorchidism, and spina bifida occulta were also noted. Hypercalcemia was not observed. Spasms were refractory to anticonvulsant drugs, but were well controlled with adrenocorticotrophic hormone (ACTH) therapy from 7 to 9 months. Mental development was severely retarded. At 21 months, he could not crawl or sit, and his developmental quotient (DQ) was 20. Abdominal ultrasonography, auditory brainstem response, and fundoscopy did not reveal any abnormality. Brain magnetic resonance imaging (MRI) implied atrophic brain (Supporting Information Fig. S1), which may have been caused by ACTH therapy.

Patient 2. A girl was born by normal vaginal delivery at term with a body weight of 2,600 g. Because of a moderate systolic murmur, she was examined, and cardiac hypertrophy and a prominent thick cardiac muscle were revealed by chest-X-ray and echocardiography (Supporting Information Figs. S2A, B), respectively. Heart catheterization revealed supravalvular aortic stenosis, peripheral pulmonary stenosis (Supporting Information Figs. S2C, D) and high pressure at 99 mmHg, 80 mmHg, 20 mmHg, and 39 mmHg, in the left ventricle, aorta, pulmonary artery, and right ventricle, respectively. She was treated with β-blockers without any arrhythmia and exacerbation of hypertrophic cardiomyopathy. She had characteristic facial features, with a wide large mouth and an elfin face. Conventional FISH analysis showed microdeletions in 7q11.23 (data not shown). At 18 months, she suffered serial tonic spasms more than 30 times per day. Electroencephalogram showed typical hypsarrhythmia (Supporting Information Fig. S2E) and MRI revealed normal structure and signal intensities in the brain (Supporting Information Figs. S2F, G). We first prescribed several antiepileptic drugs (i.e., sodium valproate, zonisamide and carbamazepine in turn), but these failed to decrease her epileptic attacks. Finally, we introduced ACTH therapy after obtaining informed consent from her parents. ACTH therapy provided successful control of her epileptic spasms, although some exacerbation of cardiac hypertrophy was observed.

Molecular Cytogenetic Analysis of Deletions

Because infantile spasms is a very rare complication for WBS patients, the deletion breakpoints of patient 1 and patient 2 were analyzed by aCGH.

In patient 1, BAC aCGH identified losses of genomic copy numbers of eight clones (Fig. 1A). Additional FISH analysis confirmed a 5.7-Mb deletion from RP11-134N6 to RP11-204E14 (UCSC Genome Browser assembly on Mar. 2006: nucleotides 68,597,691–74,341,149; Fig. 1B,C and Table 1). The deletion was not identified in the patient's parental chromosomes (data not shown) and included the common deletion region. The telomeric deletion breakpoint was localized to RP11-600I23, which exhibited weaker signal intensity on the deleted chromosome than on normal chromosome 7 (Fig. 1C). RP11-600I23 was exactly matched to telomeric LCR. No LCR-related structures were identified around the proximal deletion breakpoint.

In patient 2, oligo aCGH revealed a microdeletion of 7q11.23-q11.23 with a deletion size of 4.1-Mb (72,338,350-76,475,408; Fig. 2A,B). Two-color FISH analysis confirmed the deletion by the loss of the probe signal (Figs. 2C,D, Table 1).

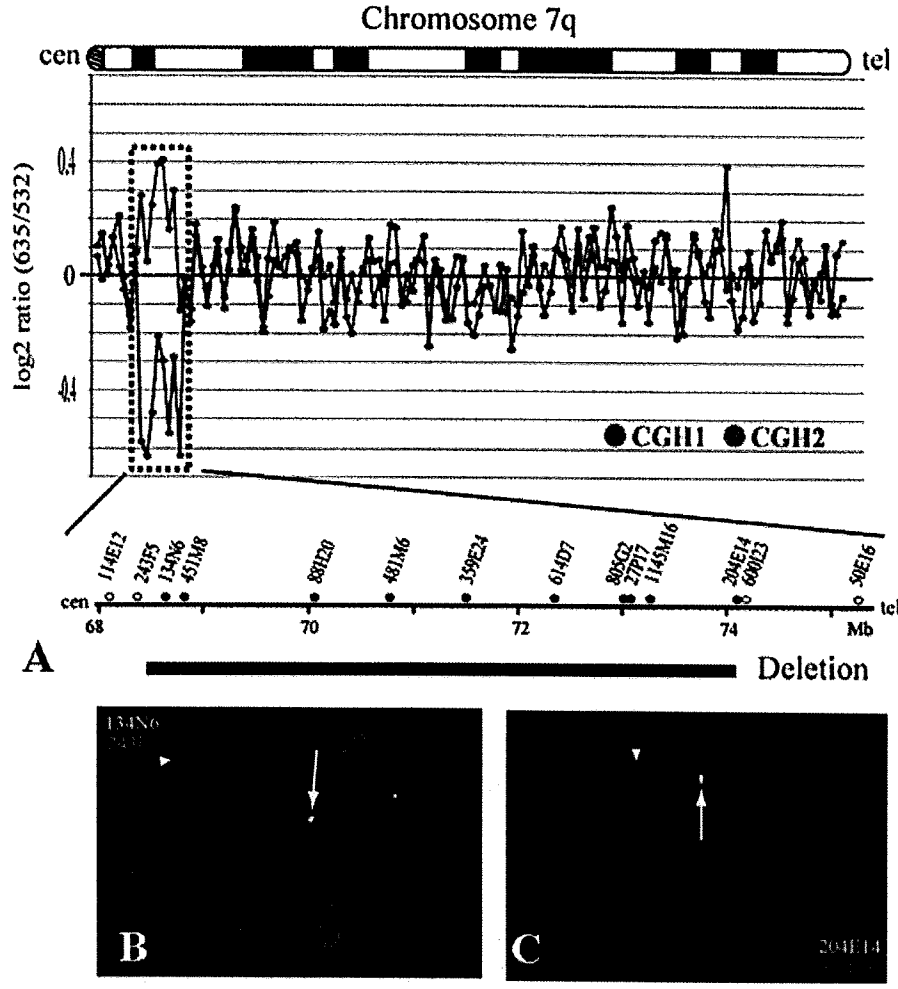

FIG. 1. Molecular cytogenetic analysis of the deletion of 7q11.23 in patient 1 using BAC aCGH and FISH analyses. **A:** aCGH analysis of chromosome 7q. Results are presented below the ideogram of 7q. Patient DNA labeled with Cy5 and normal control DNA labeled with Cy3 was used to obtain the CGH1 data (red), and the CGH2 data (green) was obtained using the same DNAs with the dye labels reversed. The dashed box indicates deleted clones, and is expanded below to give detailed information of the BAC clones used in this study (UCSC Genome Browser coordinates, build 36). Filled circles represent deleted BACs, and open circles represent clones that were not deleted. **(B, C)** Chromosomal FISH analyses. Arrows depict visible signals and arrowheads depict absence of signal.

Identification of Zebrafish *hip1*

Although several genes exist in the expanded deletion region of chromosome 7q11.23 in patient 2, there are two candidate genes normally expressed in the brain and therefore potentially responsible for the observed symptoms; i.e. tyrosine 3-monooxygenase/tryptophan 5-monooxygenase activation protein, gamma (14-3-3gamma; YWHAG) gene and the huntingtin-interacting protein 1 (HIP1) gene.

To study whether the deletion of these loci have any relation to infantile spasms and cardiomegaly, we used zebrafish as a model organism. In zebrafish, a homolog of mammalian *HIP1* has yet to be experimentally isolated, but its sequence has been predicted from genomic information. Therefore, for functional analysis, we cloned and identified the cDNA encoding zebrafish *hip1*. Using a reverse transcription (RT)-polymerase chain reaction (PCR)-based strategy, we obtained a full-length open reading frame (ORF) of zebrafish *hip1*, consisting of 3,141 bases and encoding 1,047 amino acids (Accession #AB494966). Zebrafish Hip1 protein has 70% identity to its human and mouse homologs. In addition, in silico software pfam analysis (http://pfam.sanger.ac.uk) revealed that zebrafish *Hip1* contains an N-terminal ANTH/ENTH domain and a C-terminal I/LWEQ domain, both of which are conserved in human *HIP1* (Bhattacharyya *et al.*, 2008). Collectively, these results suggest that *hip1* identified in this study is the zebrafish homolog of mammalian *HIP1* structurally and functionally.

Table 1
Summary of FISH Analyses

BAC clone	Coverage	Location			Patient 1	Patient 2
		Band	Start	End		
RP11-114E12		7q11.22	68,036,962	68,208,211	no deletion	
RP11-243F5		7q11.22	68,389,193	68,579,447	no deletion	
RP11-134N6	*AUTS2*	7q11.22	68,597,691	68,766,491	del	
RP11-88H20		7q11.22	70,101,386	70,101,595	del	
RP11-481M6	*CALN2*	7q11.22	70,766,345	70,944,325	del	
RP11-193J17		7q11.22	71,257,317	71,371,995		marker
RP11-359E24		7q11.22	71,495,966	71,682,413	del	
RP11-479C13		7q11.23	71,883,286	72,073.394		no deletion
RP11-396K3		7q11.23	71,903,765	72,538,417		no deletion
RP11-483G21		7q11.23	72,326,667	72,513,882		del
RP11-614D7		7q11.23	72,375,570	72,564,868	del	
RP11-622P13	*STAX1A*	7q11.23	72,639,987	72,819,209		del
RP11-805G2		7q11.23	73,047,721	73,249,220	del	
	ELN	7q11.23	73,080,363	73,122,172		
RP11-27P17	*LIMK1*	7q11.23	73,122,968	73,290,039	del	
RP11-7M12		7q11.23	73,249,265	73,431,303		del
RP11-1145M16		7q11.23	73,330,134	73,491,216	del	
RP11-247L6		7q11.23	73,510,529	73,676,067		del
RP11-137E8		7q11.23	73,528,656	73,767,523		del
RP11-201E14		7q11.23	74,108,105	74,267,152	del	
RP11-600I23		7q11.23	74,240,609	74,341,149	del	
RP11-99J9	*HIP1*	7q11.23	74,964,894	75,145,939		del
RP11-845K6		7q11.23	75,055,521	75,239,517		del
RP11-50E16		7q11.23	75,362,579	75,520,752	no deletion	
RP11-229D13		7q11.23	75,401,774	75,583,095		del
RP11-951G4	*YWHAG*	7q11.23	75,607,193	75,807,597		del
RP11-340A14		7q11.23	75,968,235	76,028,838		del
RP11-87O14		7q11.23	76,306,441	76,490,214		del
RP11-467H10		7q11.23	76,490,656	75,587,315		no deletion

Genome location corresponds to the March 2006 human reference sequence (NCBI Build 36).
del: deletion

For functional analysis of zebrafish *hip1*, we chose a gene knockdown strategy using morpholino antisense oligos (MOs). Because this approach requires precise nucleotide sequence information of the 5′-untranslated region (UTR), we performed 5′ rapid amplification of cDNA ends (RACE) to determine the sequence of the 5′-UTR of *hip1* in our zebrafish strain. Several nucleotide fragments, ranging from 121 to 264 bases, corresponding to the region upstream of the translation initiation ATG codon were obtained. The 121-base overlapping sequence of these clones was completely identical, and was of sufficient length to design two nonoverlapping, translation-inhibiting MOs (*hip1*-MO1 and *hip1*-MO2). A 5′-terminal guanine residue on the longest clone, rather than the observed thymine in the genomic sequence, suggested that this 264-bp clone contained the full-length 5′-UTR (Supporting Information Fig. S3). In addition, 386 bases of the 3′-UTR, including the polyadenylation signal and polyA tail, were also cloned. Overall, we identified the complete cDNA sequence of zebrafish *hip1*.

Sequence Analysis of 5′-UTR and Exon-Intron Junctions of Zebrafish *ywhag1*

Although a zebrafish homolog of human *YWHAG* was previously isolated and reported as *ywhag1* (Besser *et al.*, 2007; Pujic *et al.*, 2006; Woods *et al.*, 2005), the 5′-UTR in our zebrafish strain had to be determined to design MOs against zebrafish *ywhag1*. 5′ RACE revealed variation of sequence and length, ranging from 29 to 160 bases, in the 5′-UTR of *ywhag1*. Because the 5′ terminus of the shortest clone contained a guanine residue rather than the adenine residue identified in the other clones, this clone was identified as a full-length clone of the shortest form of the 5′-UTR (Supporting Information Fig. S4). To maximize the effect of the MOs, this shortest sequence was used as a template to design MOs that bind all transcripts of *ywhag1*.

Because the 5′-UTR we cloned was too short and not suited for MO binding, we obtained only one MO for translational inhibition of this gene (*ywhag1*-MO1). Because we needed another MO for splicing inhibition, genomic sequences at exon–intron boundaries were required. However, the whole sequence of *ywhag1* was splitted into two clones, Zv7_NA122 and Zv7_NA727, representing the 5′-terminal region (consisting of the 5′-UTR and the 5′ portion of the ORF [initiator ATG to 87G]) and the 3′-terminal region (the 3′ portion of the ORF [88G to the stop codon] and the 3′-UTR), respectively. According to the information in these sequences, zebrafish *ywhag1* was revealed to be composed of two exons and one intron (Supporting Information Fig. S5). Consequently, we cloned fragments containing the puta-

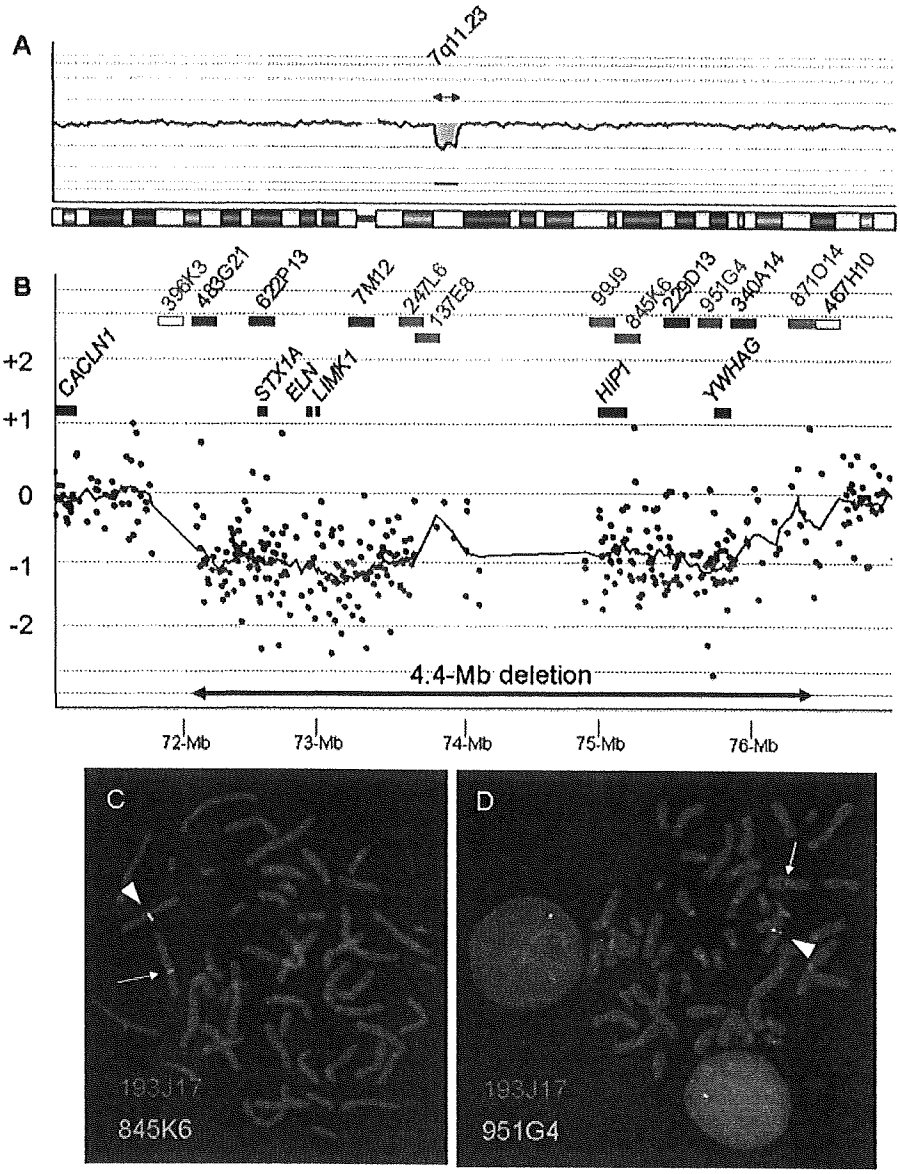

FIG. 2. Molecular cytogenetic analysis of the deletion of 7q11.23 in patient 2 using oligo array CGH and FISH analyses. **A:** Chromosome view indicating loss of genomic copy number in 7q11.23. **B:** Gene View indicating the range of the 4.1-Mb deletion (double-headed arrow, bottom). Black rectangles indicate the locations of known genes within the deletion region. Red and green rectangles indicate the locations of the BAC clones used for FISH analyses. Closed and open rectangles indicate deletion and no deletion, respectively. (C, D) FISH analyses indicating deletion of the green signals (arrows) of RP11-845K6 (C) and RP11-951G4 (D).

tive junction of exon 1/intron 1 and intron 1/exon 2 (Supporting Information Fig. S5), and designed *ywhag1*-spMO.

Zebrafish hip1 Plays No Obvious Role in Brain Development

To confirm whether the deletion of *HIP1* contributes to the phenotype of patient 2, we performed gene knockdown analysis of *hip1* in zebrafish. Microinjection of a small amount (3 ng) of *hip1*-MO1 reduced the yolk extension without any other remarkable phenotypes (Fig. 3E,F) compared with wild type and control MO-injected zebrafish (Fig. 3A–D). By a high dose (5 ng) injection of *hip1*-MO1, the morphants showed complete absence of yolk extension, a narrow body along the dorsoventral axis, and mandibular hypoplasia (Fig. 3G,H). To verify whether these phenotypes were specific for

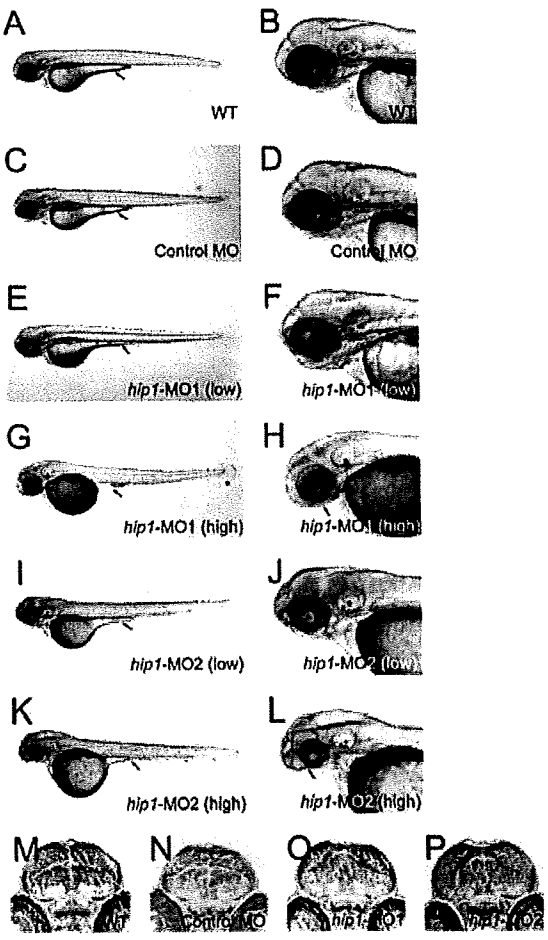

FIG. 3. Zebrafish *hip1* has no evident role in brain development. Morphological observation of wild type (WT) (**A, B**), control (**C, D**), *hip1*-MO1 morphant (E, F, G, H), and *hip1*-MO2 morphant (**I, J, K, L**) embryos at 72 hpf. Gene knockdown of *hip1* using a low dose (3 ng) of MOs caused reduction of yolk extension (arrow in A, C, **E, I**), whereas a high dose (5 ng) resulted in complete lack of yolk extension, narrow body width, and mandibular agenesis (**G, H**, K, L). Arrows indicate yolk extension (G, K) and diminished lower jaw (H, L). Cross-sections of the midbrain in wild type (**M**), control (**N**), *hip1*-MO1 morphant (**O**) and *hip1*-MO2 morphant (**P**) embryos at 72 hpf. All images are displayed with dorsal to the top; A-L are displayed with rostral to the left.

knockdown of *bip1*, the other translation-inhibiting MO, *bip1*-MO2, was used. Similar to *bip1*-MO1 morphants, *bip1*-MO2 morphants showed dose-dependent phenotypes, including reduced yolk extension with no other defects when 3 ng of *bip1*-MO2 was injected (Fig. 3I,J), and complete absence of yolk extension, narrow body along the dorsoventral axis, and severe mandibular aplasia when 5 ng of *bip1*-MO2 was injected (Fig. 3K, L). In addition to these common phenotypes, *bip1*-MO2 morphants also displayed dysplasia of the brain with low penetrance at the higher dose (Fig. 3L), suggesting that this cerebral defect was not the result of specific action of *bip1* knockdown. To examine this, we prepared serial cross-sections of the head of both morphants treated with the low MO dose. If *bip1* had any primary function in brain development, some sort of alteration would likely have occurred in the brain of morphants following injection of a low dose of *bip1* MOs. Although whole brains (from the prosencephalon to the rhombencephalon and along the anteroposterior axis) of embryos at 72 hours post-fertilization (hpf) were cut into serial sections and compared each other, no differences between morphants and wild type or control embryos were observed in any area of the brain (e.g., Fig. 3M–P; corresponding to middle of midbrain). These results indicate that gene knockdown of *bip1* has no obvious effect on the developing brain, although the possibility of involvement of *bip1* was not completely omitted.

Zebrafish ywhag1 Contributes to Brain and Heart Development

It has been reported that, during embryonic development of zebrafish, *ywhag1* is expressed in the head, especially in the diencephalon, tegmentum, and hindbrain (Besser *et al.*, 2007). This expression pattern suggests possible functions of this gene in cerebral and neural growth. Therefore, to investigate whether *ywhag1* has a role in brain development or any relationship to the symptoms of patient 2, we performed gene knockdown of *ywhag1*. Compared with wild type and control embryos (Fig. 4A–D), the *ywhag1*-MO1 morphants (Fig. 4E,F) showed hypomorphic heads and enlarged heart tubes, whereas trunk development was not affected. To confirm that these defects were caused by *ywhag1* knockdown, the splice-inhibiting *ywhag1*-spMO was used. Microinjection of *ywhag1*-spMO drastically reduced mRNA level of *ywhag1* (Supporting Information Fig. S6), and resulted in morphants with a severely hypomorphic head phenotype and enlargement of the heart tube (Fig. 4G,H) similar to *ywhag1*-MO1 morphants (Fig. 4E,F). To gain more confidence, we tested whether coinjection of two MOs at low levels elicits synergistic effect. The quarter amount of each MO (0.75 ng of *ywhag1*-MO1 and 1 ng of *ywhag1*-spMO) that did not cause any obvious defects (data not shown) was coinjected into embryos. Morphant coinjected with these two MOs (*ywhag1*-spMO1+spMO) showed similar phenotypes common to *ywhag1*-MO1- and *ywhag1*-spMO-morphants (Fig. 4I,J). This result indicated that these two MOs exerted the synergistic effect in coinjected embryos (*ywhag1*-spMO1+spMO), and that *ywhag1* is required for normal development of the brain and the heart.

For further investigation of the brain and the heart aberrations in the morphant embryos, serial sections of the head and the heart were examined. Based on the expression pattern of *ywhag1*, we focused on the brain sections containing the diencephalon and midbrain tegmentum (Besser *et al.*, 2007). Compared with wild type and control embryos (Fig. 4K–N), *ywhag1* morphants

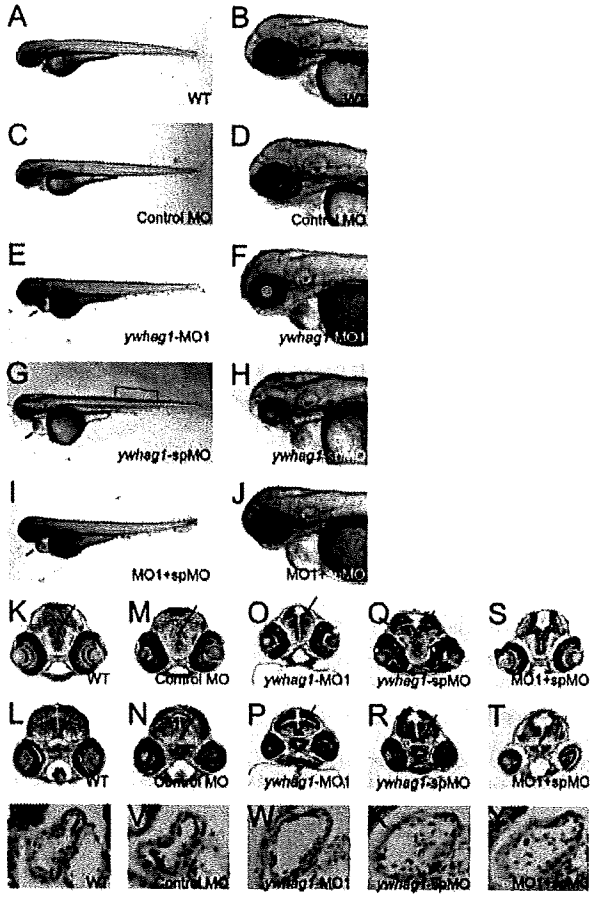

FIG. 4. Zebrafish *ywhag1* is required for development of the brain and the heart. Morphological observation of wild type (WT) (**A**, **B**), control MO morphant (**C**, **D**), *ywhag1*-MO1 morphant (E, F), *ywhag1*-spMO morphant (**G**, **H**) and *ywhag1*-MO1+*ywhag1*-spMO morphant (**I**, **J**) embryos at 72 hpf. Gene knockdown of *ywhag1* caused developmental abnormalities of the head and the enlarged heart tube. Three types of *ywhag1* morphants showed hypomorphic head (**E–J**). Although weak malformation of the trunk and the tail were observed only in *ywhag1*-spMO morphants (bracket) (G), this anomaly was likely to be nonspecific. As same as this manner, the reason of enlargements of the heart pericardiums observed in *ywhag1* morphants (arrows) (E, G, I) is obscure. Cross-sections containing the diencephalon (**K**, **M**, **O**, **Q**, **S**) and the midbrain tegmentum (**L**, **N**, O, **R**, **T**) of WT (K, L), control (M, N), *ywhag1*-MO1 morphant (O, **P**) and *ywhag1*-spMO morphant (Q, R) and *ywhag1*-MO1+spMO morphant (S, T) embryos at 72 hpf are shown (arrows). Compared with WT (K, L) and control (M, N), *ywhag1* morphants showed hypomorphic heads. Cross-sections of the heart ventricles in WT (**U**), control (**V**), *ywhag1*-MO1 morphant (**W**), *ywhag1*-spMO morphant (**X**) and *ywhag1*-MO1+spMO morphant (**Y**) embryos at 72 hpf. Compared with WT (U) and control (V), *ywhag1* morphants (W, X, Y) showed enlarged ventricles of the hearts. All images are displayed with dorsal to the top; A-J are displayed with rostral to the left.

exhibited obvious dysplasia of the brain (Fig. 4O–T). In normal cerebral development in the zebrafish, the brain ventricle is narrowed along with the progression of development and almost buried until 72 hpf (Fig. 4K–N). In the knockdown experiments, wild type and control embryos had a solid diencephalon structure (Fig. 4K,M), whereas the diencephalons of all *ywhag1* morphants were divided by the brain ventricle (Fig. 4O,Q,S). Similar abnormal partitions were observed in the tectum opticum (the dorsal upper structure of midbrain tegmentum indicated by arrow; Fig. 4P,R,T). Furthermore, the midbrain tegmentum was not formed properly in morphants (Fig. 4P,R,T). About the heart tube, major diameter of the ventricle was obviously enlarged in *ywhag1* morphants (Fig. 4W,X,Y) compared with wild type and control morphants (Fig. 4U,V). These results strongly indicate that *ywhag1* is important for normal brain and heart development.

Regarding the functions of the heart in all zebrafishes, we measured the pulse rate, and there were no statistically significant differences among all groups of larvae. However, incidence of arrhythmia was significantly elevated in all three types of *ywhag1* morphants (Supporting Information Table S1 and Fig. S7).

Mutation analysis of *HIP1* and *YWHAG* in Patients With Neurological Symptoms

Although total of 142 samples derived from patients with neurological symptoms including developmental delay and/or epilepsy were analyzed for mutation analysis of *HIP1* and *YWHAG*, there was no pathogenic mutation.

DISCUSSION

Because WBS is not usually associated with infantile spasms, genotype-phonotype comparisons in WBS patients with atypically large deletions may assist identification of gene(s) responsible for infantile spasms. Marshall *et al.* (2008) investigated 16 patients associated with documented seizures and interstitial deletions of 7q11.23-q21.1, which is neighboring to the WBS critical region, and revealed overlapping deletions of the *MAGI2* in most patients. However, they reported at least one patient having infantile spasms and a chromosomal deletion including WBS critical region but in which *MAGI2* was not included, who had been reported previously by Morimoto et al. (2003).

In this study, we identified two additional WBS patients with atypically large deletions. Patient 1 had a deletion at 7q11.23 that extended into the proximal region and included three genes; i.e. *AUTS2*, *WBSCR17*, and *CALN1* (Fig. 5, Table 1). Expression of human *CALN1* (*calneuron 1)* is brain specific (Wu *et al.*, 2001), and expression of the mouse homolog in the cerebellum increases from the postnatal 2nd week to day 21, and reaches to adult level. In situ hybridization showed a high level of expression of *CALN1* in the cerebellum, hippocampus, striatum, and cortex (Wu *et al.*, 2001). The postnatal expression pattern in mice is consistent with the onset of infantile spasms in humans, which occurs from 3 to 6 months after birth. *CALN1* shows sig-

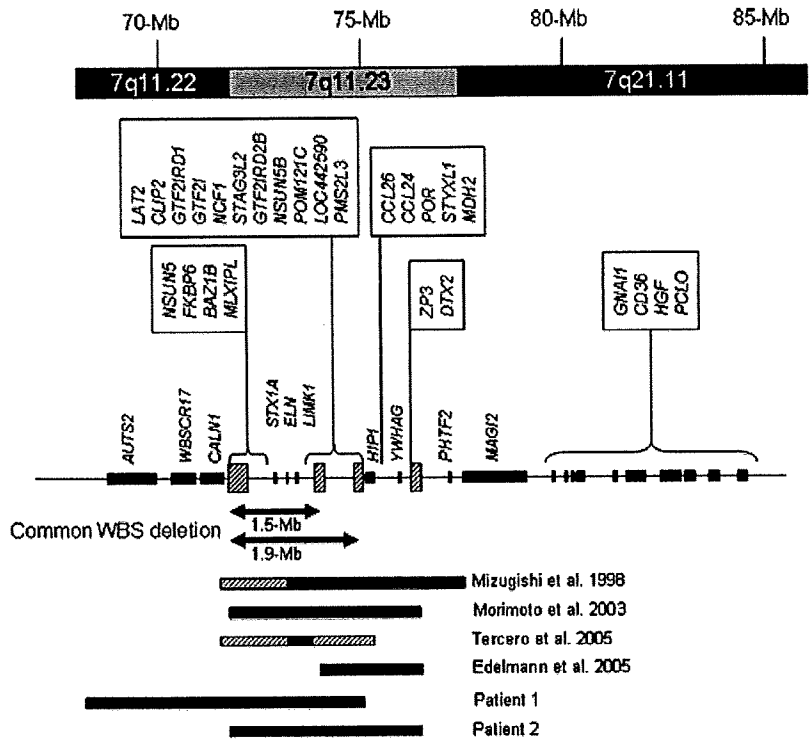

FIG. 5. Chromosome map around the common WBS deletion. Black and hatched rectangles on a horizontal bar indicate the sizes and the locations of genes and duplicated segments, respectively. Gray bars indicate the region of the chromosome deleted in the indicated patient, with the ambiguity indicated as hatched bars.

nificant similarity to members of the calmodulin superfamily (Wu *et al.*, 2001). Thus, haploinsufficiency of *CALN1* may cause the infantile spasms in this patient. *AUTS2* is also a compelling candidate gene for the infantile spasms in patient 1, because it is robustly expressed in the fetal brain and is reported to be interrupted by a translocation breakpoint in patients with autistic behavior or mental retardation (Kalscheuer *et al.*, 2007; Sultana *et al.*, 2002).

Patient 2 had a deletion that extended into the distal telomeric region. The range of this deletion is exactly same as that of the patient reported by Morimoto *et al.* who also showed infantile spasms and cardiomegaly (Morimoto *et al.*, 2003) (see Fig. 5). At the telomeric breakpoint, there is a region of duplicated segments. This telomeric breakpoint was also shared by a patient reported by Edelmann *et al.* (2007), who presented with autism associated with a chromosomal deletion of 7q11.23, which did not include *ELN* but expanded into the telomeric region beyond the WBS critical region (see Fig. 5). These common breakpoints indicate that this region of duplicated segments can act as a LCR for nonhomologous allele recombination (NHAR).

There are 9 genes in the expanded deletion toward the telomeric region neigboring the WBS critical region (see Fig. 5). Among them, Edelmann *et al.* (2007) focused on *HIP1* and *YWHAG* as the prime candidates responsible for autism seen in their patient, and analyzed the expression levels of them by RT-PCR method. Then, they revealed reduced expression of *YWHAG* in transformed lymphocytes derived from the patient, but no decrease in *HIP1*. Based on these findings, we analyzed the function of *HIP1* and *YWHAG* using a gene knockdown system in zebrafish, and the correlation with neurological functions.

In this study, the zebrafish *hip1* knockdown did not show significant abnormality, which is consistent with previous reports of *Hip1*-deficient mice. Homozygous *Hip1-/-* mice generated by targeted deletion exhibited degeneration of the seminiferous tubules of the testis with excessive apoptosis of postmeiotic spermatids, but these mice developed to adulthood and did not show overt neurologic symptoms (Rao *et al.*, 2001). In addition, mice with different deletions of *hip1* showed hematopoietic abnormalities, spinal defects, and cataracts due to cell death in the lens, but had no notable cerebral or neurological anomalies (Oravecz-Wilson et al., 2004).

In contrast, reduced brain size and enlargement of the heart tube were observed when *ywhag1* was knocked down in zebrafish. This indicates that the infantile spasms and the cardiomegaly observed in patient 2 might be derived from haploinsufficiency of *YWHAG*,

because the WBS patient reported by Morimoto *et al* (2003). also showed infantile spasms and cardiomegaly. *YWHAG* binds to *protein kinase C alpha (PRKCA) and p53* is directly phosphorylated by *PRKCA*, which is crucial for activation of *p53 protein* (Autieri and Carbone, 1999; Price and Youmell, 1997). 14-3-3 proteins including *YWHAG* modulate cell survival and control apoptosis (Morrison, 2009; Porter *et al.*, 2006) and inhibition of physical binding between 14-3-3 and its ligand proteins causes apoptosis (Masters and Fu, 2001). Therefore, the etiology of hypoplastic brain in the zebrafish model might be the consequence of apoptic cell death in central nervous system at early development. Regarding the involvement of the heart, we observed arrhythmia in *Ywhag1* knockdown zebrafish and the incidence of arrhythmia in *ywhag1* knockdown zebrafish is worth noting. Although patient 2 did not show arrhythmia, it might be masked by medication with beta-blockers. Since we did not identify any mutations in patients with mental retardation and/or epilepsy, no definitive evidence of a link between *HIP1/YWHAG* haploinsufficiencies and neurological symptoms was obtained. However, given the evidence reported herein, *YWHAG* are promising candidate genes for infantile spasms.

In conclusion, we have described two new WBS patients that presented with infantile spasms and had atypically large deletions in 7q11, one extending into the proximal side of the common WBS deletion and one extending into the telomeric side. In the telomeric side, we identified two promising candidate genes, *HIP1* and *YWHAG*. Using a knockdown approach, we showed that a loss of zebrafish *ywhag1* leads to brain development delay and heart tube enlargement. Because the patient with haploinsufficiency of *YWHAG* showed infantile spasms and cardiomegaly, *YWHAG* may have important roles in both brain and heart development. Although there was no *YWHAG* mutation identified in the patients with mental retardation and/or epilepsy, this gene is a noteworthy candidate for epilepsy, along with *AUTS2*, *CALN1*, and *HIP1*.

MATERIALS AND METHODS

Subjects

After obtaining informed consents based on a permission approved by the institution's ethical committee, peripheral blood samples were obtained from the patients and their parents.

For genomic mutation screening for *HIP1* and *YWHAG*, we used 142 DNA samples derived from 128 and 14 patients with idiopathic mental retardation with and without epilepsy, respectively. Etiologies of all these patients were unknown and were negated to have genomic copy number aberrations using aCGH (Shimojima *et al.*, 2009b). In 128 patients with epilepsy, there were 5 patients with early infantile epileptic encephalopathy, 43 patients with West syndrome, and 2 patients with Lennox-Gastaut syndrome. All of the 14 nonepileptic patients showed cerebral dsygenesis including gyrus malformation, brain atrophy, and microcephaly.

aCGH Analysis

For aCGH analysis of patient 1, we used the originally developed microarray in which 5,057 BAC/PAC clones were plotted. We selected probes using the UCSC Genome Browser (http://genome.ucsc.edu) spaced every 0.7 Mb across the whole human genome, and chose 4,235 clones that showed a unique FISH signal at the predicted chromosomal location. A total of 822 clones were not subjected to aCGH analysis; 438 (8.7%) yielded multiple chromosomal signals using FISH and 384 (7.6%) showed aberrant FISH signals likely due to contamination in our laboratory. Fifty-nine BAC/PAC clones, previously used for subtelomere and syndromic-MR-specific microarray analysis, were among the 4,235 clones (Harada *et al.*, 2004; Kurosawa *et al.*, 2004). BAC/PAC DNA was extracted using the PI-100 automatic DNA extraction system (Kurabo, Osaka, Japan), subjected to two rounds of PCR amplification, purified, adjusted to a final concentration of >500 ng/μl, and spotted in duplicate on CodeLinkTM activated slides (Amersham Biosciences Corp, Piscataway, NJ) using the ink-jet spotting method (Nihon Gaishi, Nagoya, Japan) as described previously (Miyake *et al.*, 2006). aCGH analysis was performed using 4,235 BAC arrays. After complete digestion using *DpnII*, CGH1 was set up using subject DNA labeled with Cy-5-dCTP (Amersham Biosciences) and reference DNA labeled with Cy-3-dCTP (Amersham Biosciences) using a DNA random primer kit (Invitrogen, Carlsbad, CA). To rule out false positives, dyes were swapped in the CGH2 set (subject DNA was labeled with Cy3 and reference DNA was labeled with Cy5), such that the signal patterns of CGH1 were reversed. Prehybridization and hybridization were performed as described previously (Harada *et al.*, 2004). The arrays were scanned by GenePix 4000B (Axon Instruments, Union City, CA) and analyzed using GenePix Pro 6.0 (Axon Instruments). The signal intensity ratio between subject and control DNA was calculated from the data of the single-slide experiment in each for CGH1 and CGH2, using the ratio of means formula (F635 Mean-B635 Median/F532 Mean-B532 Median) according to GenePix Pro. 6.0. The standard deviation of each clone was calculated. The signal intensity ratio was considered significant if it was greater than three standard deviations from the mean in both the CGH1 and CGH2 sample sets.

For patient 2, genomic copy number aberrations were analyzed using the Human Genome CGH Microarray 105A chip (Agilent Technologies, Santa Clara, CA) according to methods described elsewhere (Shimojima *et al.*, 2009a). Briefly, 500 ng genomic DNA was extracted from peripheral blood of the patient and the reference individual, using the QIAquick DNA extraction kit (QIAgen, Valencia, CA), and was digested with restriction enzymes. Cy-5-dUTP (patient) or Cy-3-dUTP (reference) was incorporated using the Klenow frag-